CrossMark

ORIGINAL

Tieding Guo · Houjun Kang · Lianhua Wang · Yueyu Zhao

Cable's non-planar coupled vibrations under asynchronous out-of-plane support motions: travelling wave effect

Abstract Cable's non-planar coupled dynamics under asynchronous out-of-plane support motions is investigated in this paper. The moving boundary difficulty is coped by transforming the small support motions into two resonant boundary modulation terms, and cable's one-to-one resonant coupled non-planar dynamics is reduced through attacking directly the continuous dynamic equations by the multiple scale method. Two boundary dynamic coefficients are derived, characterizing the boundary modulation effects, which are equal for symmetric out-of-plane modes, while opposite for asymmetric ones. Both cable's frequency and amplitude (of support deflection) response diagrams, with phase lags between supports, are constructed using numerical continuation algorithms, and the steady-state solutions' stability and bifurcation properties are determined, based upon which the phase lags' effects on dynamic responses, or travelling wave effects, are thoroughly investigated, through varying the phase lags.

Keywords Cable dynamics · Asynchronous support excitations · Travelling wave effect · Multiple scale method

1 Introduction

Elastic cables, as long-span structure members, are widely used in structure engineering [1–7], such as long-span suspension or stay-cable bridges, cross-sea or cross-valley power transmission lines. Furthermore, due to increasing usage of CFRP (carbon fibre-reinforced polymers) [8], the cable's span is extended to over 1000 (m) and is still soaring significantly in the recent years.

Cable's dynamic behaviours are complicated and extensive investigations have been conducted by many researchers in the past few decades [1–7]. Irvine and Caughey [3,4] proposed a linear cable model and gave linear modal results, and Triantafyllou [5] focused on dynamics of mooring cables. Using single-degree-of-freedom (sdof) cable models, Hagedorn and Schäfer [9], Luongo et al. [10], Benedettini and Rega [11] studied nonlinear oscillations of elastic cables.

Support motions-induced boundary excitation is one of the main excitation sources for engineering cables. Using Galerkin discretization and the multiple scale method, Perkins [12], Benedettini et al. [13] studied cable dynamics under support motions. Note that the main difficulty associated with moving supports is cable's linear mode analysis with moving boundary conditions. In this respect, Perkins [12] used the classical cable modes under fixed supports, and Benedettini et al. [13] introduced a quasi-static mode assumption and decomposed the cable's mode into two components, i.e. the linear quasi-static component caused by the moving support, and the small oscillating component under fixed supports. Although this quasi-static mode concept is approximate

T. Guo (✉) · H. Kang · L. Wang · Y. Zhao
College of Civil Engineering, Hunan University, Changsha 410082, Hunan, People's Republic of China
E-mail: guotd@hnu.edu.cn

or empirical, the method and similar strategies thereafter are regarded pragmatic and are widely used for studying cable dynamics caused by moving decks/towers [14–21].

A boundary modulation approach, formulated by the authors in Ref. [22], can be used to cope with cable's dynamic boundary difficulty under support excitations. The basic idea is rather simple, i.e. the support motion's order/scale is assumed to be smaller than that of the cable, and the moving supports can be treated as perturbation terms. Thus, through attacking directly the continuous dynamic equations using the multiple scale method, the resonant support motions are transformed into boundary modulation terms for cable's reduced (slow) dynamics. This key idea, i.e. regarding small boundary/support motions as perturbations and transforming them into modulation terms on the main structure, was also used by Shaw and Pierre [23], Nayfeh [24], Pakdemirli and Boyaci [25].

For multiple support excitations, the situation would be more complex. A peculiar and important factor, especially for long or super-long cables, is the asynchronous support excitations caused by seismic loadings. Explicitly, the time taken for seismic waves travelling across cable's two widely spaced supports, say l/v, is finite and thus not negligible [17,26]. This is also called a travelling wave effect. In other words, the multiple support excitations would be asynchronous and the phase lag/shift between the support motions is not zero. Therefore, the phase lag's effect on long-cable's dynamics should be carefully modelled and analysed.

Based upon the basic boundary modulation formulation established in Ref. [22], this paper focuses on cable's non-planar coupled dynamics under asynchronous out-of-plane support motions. In this respect, with damping neglected, Ref. [17] proposed a Galerkin discretized model for non-resonant coupled dynamics and used the empirical quasi-static motion assumption mentioned above. As pointed out in references [27–29], directly reduced models obtained through directly attacking cable's continuous dynamic equations by the multiple scale method would be more appropriate than the Galerkin discretized models [29].

Thus, our paper's first aim would be to establish a boundary modulation formulation for long-cable's dynamic modelling and analysis under multiple asynchronous support motions, thus extending the boundary modulation formulation in Ref. [22] to multiple support cases. The second aim would be to analyse the phase lag's effects on cable's non-planar coupled dynamic responses, and we would mainly focus on one-to-one in-plane and out-of-plane resonant coupled interactions.

2 Problem statement

A homogenous, elastic cable, is horizontally hanged at oscillating supports O and A (for example, bridge decks or towers in suspension/stay-cable bridge systems), as depicted in Fig. 1. The cable stretches in a quasi-static manner, i.e, the longitudinal dynamic time scale is much smaller (thus fast) than the vertical one [30], we present the dimensionless governing equations for cable's non-planar motions [27,28]:

$$\ddot{w} + 2c\dot{w} - w'' - \alpha\left(w'' + y''\right)\int_0^1 \left(y'w' + \frac{1}{2}w'^2 + \frac{1}{2}v'^2\right)\mathrm{d}x = 0 \tag{1}$$

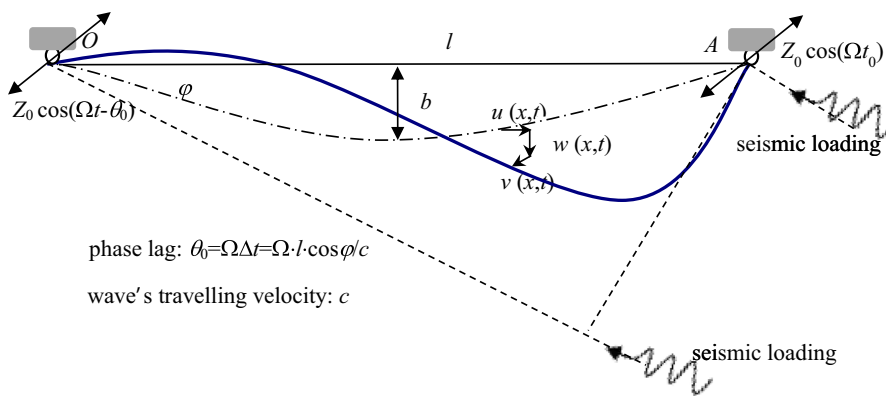**Fig. 1** Cable's non-planar coupled motions under asynchronous out-of-plane support excitations: travelling wave effect and the phase lag θ_0

$$\ddot{v} + 2c\dot{v} - v'' - \alpha v'' \int_0^1 \left(y'w' + \frac{1}{2}w'^2 + \frac{1}{2}v'^2 \right) dx = 0 \tag{2}$$

Here cable's in-plane vertical displacements, and out-plane displacements, are denoted by $w(x,t)$ and $v(x,t)$, respectively. The longitudinal displacement $u(x,t)$ has been kinetically condensed in Eqs. (1) and (2) (the effect of the kinetic condensation is explored in Ref. [31]). The cable's initial parabolic shape is $y(x) = 4fx(1-x)$, where $f = b/l$ is cable's sag-to-span ratio, with the initial sag and span denoted by b and l, respectively. The dimensionless stiffness is $\alpha = 8bEA/mgl^2$. The dimensionless time t and spatial coordinate x are defined as $t = t_1/T$, and $x = x_1/L$, respectively. Here $T^2 = 8b/g$, and the original time(spatial) coordinate is denoted by $t_1(x_1)$. Note that the overdot and prime above denote differentiation with respect dimensionless time t and spatial coordinate x, respectively. Further details can be found in Ref. [22].

The in-plane and out-of-plane boundary conditions are

$$\begin{array}{ll} w(x,t) = 0, & \text{at } x = 0, 1 \\ v(x,t) = Z_0 \cos(\Omega t - \Omega\Delta t) = Z_0 \cos(\Omega t - \theta_0), & \text{at } x = 0 \\ v(x,t) = z(t) = Z_0 \cos\Omega t, & \text{at } x = 1 \end{array} \tag{3}$$

We note that the out-of-plane boundary conditions at $x = 0$ and $x = 1$ are asynchronous, and the phase lag due to the travelling wave effect is $\theta_0 = \Omega\,\Delta t$, where Ω and Δt are seismic wave's frequency and travelling time between supports. The main aim of this study is to understand the phase lag's effect on cable's coupled dynamics through establishing an extended (thus more general) boundary modulation formulation.

3 Reduced modelling by the multiple scale method

For the sake of simplicity, we rewrite Eq. (1) in a first-order state space form

$$\begin{array}{ll} \dot{w} - p = 0, & \dot{p} + 2cp + L_w(w) - N_2(w,v) - N_3(w,v) = 0 \\ \dot{v} - q = 0, & \dot{q} + 2cq + L_v(v) - \tilde{N}_2(w,v) - \tilde{N}_3(w,v) = 0 \end{array} \tag{4}$$

where the linear operators L_w and L_v for in-plane and out-of-plane dynamics are

$$L_w(w) = -w'' - \alpha y'' \int_0^1 (y'w')dx, \quad L_v(v) = -v'' \tag{5}$$

And the quadratic and cubic nonlinear terms are defined as

$$\begin{array}{ll} N_2(w,v) = \alpha w'' \int_0^1 (y'w')dx + \frac{\alpha y''}{2} \int_0^1 (w'^2 + v'^2)dx, & N_3(w,v) = \frac{\alpha w''}{2} \int_0^1 (w'^2 + v'^2)dx \\ \tilde{N}_2(w,v) = \alpha v'' \int_0^1 (y'w')\,dx, & \tilde{N}_3(w,v) = \frac{\alpha v''}{2} \int_0^1 (w'^2 + v'^2)\,dx \end{array} \tag{6}$$

The multiple moving boundary conditions are

$$\begin{array}{ll} w(x,t) = p(x,t) = 0, & v(x,t) = z(t-\Delta t), q(x,t) = \dot{z}(t-\Delta t) & \text{at } x = 0 \\ w(x,t) = p(x,t) = 0, & v(x,t) = z(t), q(x,t) = \dot{z}(t) & \text{at } x = 1 \end{array} \tag{7}$$

3.1 One-to-one resonant coupled dynamics under asynchronous support motions: multi-scale expansions

Consider one-to-one resonant interaction between in-plane and out-of-plane cable modes for the coupling system in Eqs. (4)–(7). In this case, the cubic nonlinearity due to longitudinal stretching is dominant. We seek uniform asymptotic expansions of w, v as

$$\begin{array}{l} w(x,t) = \varepsilon w_1(x, T_0, T_2) + \varepsilon^2 w_2(x, T_0, T_2) + \varepsilon^3 w_3(x, T_0, T_2) \cdots \\ v(x,t) = \varepsilon v_1(x, T_0, T_2) + \varepsilon^2 v_2(x, T_0, T_2) + \varepsilon^3 v_3(x, T_0, T_2) \cdots \end{array} \tag{8}$$

where $T_i = \varepsilon^i t$. As no resonance occurs on the time scale T_1, the above asymptotic expansion is independent of T_1. To make the damping, nonlinearity and the non-homogenous boundary condition in Eq. (7) balance at

the same order, ε^3, we reorder/rescale the damping c and the support motion as $c \rightarrow \varepsilon^2 c$, $z(t) \rightarrow \varepsilon^3 z(t)$. Substituting Eq. (8) into Eq. (4), equating coefficients of like powers of ε, we obtain

Order ε:

$$D_0 w_1 - p_1 = 0, \quad D_0 p_1 + L_w(w_1) = 0$$
$$D_0 v_1 - q_1 = 0, \quad D_0 q_1 + L_v(v_1) = 0 \tag{9}$$

with the homogenous boundary conditions

$$w_1 = p_1 = 0, \quad v_1 = q_1 = 0 \quad at \ x = 0, 1 \tag{10}$$

Order ε^2:

$$D_0 w_2 - p_2 = 0, \quad D_0 p_2 + L_w(w_2) = N_2(w_1, v_1)$$
$$D_0 v_2 - q_2 = 0, \quad D_0 q_2 + L_v(w_2) = \tilde{N}_2(w_1, v_1) \tag{11}$$

with the homogeneous boundary conditions

$$w_2 = p_2 = 0, \quad v_2 = q_2 = 0 \quad at \ x = 0, 1 \tag{12}$$

Order ε^3:

$$D_0 w_3 - p_3 = -D_2 w_1$$
$$D_0 p_3 + L_w(w_3) = -D_2 p_1 - 2cp_1 + N_3^{11} + N_3^{12}$$
$$D_0 v_3 - q_3 = -D_2 v_1$$
$$D_0 q_3 + L_v(v_3) = -D_2 q_1 - 2cq_1 + \tilde{N}_3^{11} + \tilde{N}_3^{12} \tag{13}$$

with non-homogeneous 3rd-order boundary conditions/excitations

$$w_3 = p_3 = 0, \qquad at \ x = 0, 1$$
$$v_3(x, t) = \frac{Z_0}{2} e^{i\Omega T_0} e^{-i\theta_0} + cc., \quad q_3(x, t) = i\Omega v_3 \ at \ x = 0 \tag{14}$$
$$v_3(x, t) = \frac{Z_0}{2} e^{i\Omega T_0} + cc., \qquad q_3(x, t) = i\Omega v_3 \quad at \ x = 1$$

Note that the cubic nonlinearities on the order ε^3, for both in-plane and out-of-plane dynamics, consist of two distinct terms. For the in-plane case, they are

$$N_3^{11} = \frac{\alpha w_1''}{2} \int_0^1 \left(w_1'^2 + v_1'^2\right) dx,$$
$$N_3^{12} = \alpha w_1'' \int_0^1 (y' w_2') dx + \alpha w_2'' \int_0^1 (y' w_1') dx + \alpha y'' \int_0^1 (w_1' \cdot w_2' + v_1' \cdot v_2') dx \tag{15}$$

For the out-of-plane case, they are

$$\tilde{N}_3^{11} = \frac{\alpha v_1''}{2} \int_0^1 \left(w_1'^2 + v_1'^2\right) dx, \quad \tilde{N}_3^{12} = \alpha v_1'' \int_0^1 (y' w_2') dx + \alpha v_2'' \int_0^1 (y' w_1') dx \tag{16}$$

It is noted that the cubic nonlinearity terms N_3^{11} and $\tilde{N}_3^{11}$ are caused by the self-interactions of the 1st-order solutions, and they are associated with the original cubic nonlinearity, i.e. $N_3(w, v)$ and $\tilde{N}_3(w, v)$, respectively. The new cubic terms N_3^{12} and $\tilde{N}_3^{12}$, essentially, are caused by the quadratic/mutual interaction between the 1st-order and the 2nd-order solutions, and they are rooted in cable's quadratic nonlinearity $N_2(w, v)$ and $\tilde{N}_2(w, v)$.

The solutions of the first-order problem in Eq. (9) are assumed as

$$w_1 = A_n(T_2) \phi_n(x) e^{i\omega_n^{(in)} T_0} + cc., \quad p_1 = i\omega_n^{(in)} A_n(T_2) \phi_n(x) e^{i\omega_n^{(in)} T_0} + cc.$$
$$v_1 = B_m(T_2) \varphi_m(x) e^{i\omega_m^{(out)} T_0} + cc., \quad q_1 = i\omega_m^{(out)} B_m(T_2) \varphi_m(x) e^{i\omega_m^{(out)} T_0} + cc. \tag{17}$$

where $\phi_n(x)$ and $\varphi_m(x)$ are cable's n-th in-plane and m-th out-of-plane vibration modes, with the associated characteristic frequencies $\omega_n^{(in)}$, $\omega_m^{(out)}$. Further information for cable's linear mode analysis is cited in "Appendix 1".

Substituting the 1st-order solutions in Eq. (17) into the 2nd-order perturbation equations (11), we obtain the 2nd-order in-plane equations

$$
\begin{aligned}
D_0 w_2 - p_2 &= 0 \\
D_0 p_2 + L_w(w_2) &= A_n^2 e^{\mathrm{i}2\omega_n^{(\mathrm{in})} T_0} \Pi_1(x) + A_n \bar{A}_n \Pi_2(x) \\
&\quad + B_m^2 e^{\mathrm{i}2\omega_m^{(\mathrm{out})} T_0} \Pi_3(x) + B_m \bar{B}_m \Pi_4(x) + cc.
\end{aligned}
\tag{18}
$$

and the 2nd-order out-of-plane equations

$$
\begin{aligned}
D_0 v_2 - q_2 &= 0 \\
D_0 q_2 + L_v(v_2) &= A_n B_m e^{\mathrm{i}\left(\omega_n^{(\mathrm{in})} + \omega_m^{(\mathrm{out})}\right) T_0} \Pi_5(x) + A_n \bar{B}_m e^{\mathrm{i}\left(\omega_n^{(\mathrm{in})} - \omega_m^{(\mathrm{out})}\right) T_0} \Pi_6(x) + cc.
\end{aligned}
\tag{19}
$$

where the coefficients $\Pi_{\mathrm{k}}(x)$, $k = 1, 2, \ldots, 6$, are presented in "Appendix 2".

As no resonance occurs on the order ε^2, we write the 2nd-order solutions for Eq. (19) as

$$
\begin{aligned}
w_2 &= A_n^2 e^{\mathrm{i}2\omega_n^{(\mathrm{in})} T_0} \Psi_1(x) + A_n \bar{A}_n \Psi_2(x) + B_m^2 e^{\mathrm{i}2\omega_m^{(\mathrm{out})} T_0} \Psi_3(x) + B_m \bar{B}_m \Psi_4(x) + cc. \\
v_2 &= A_n B_m e^{\mathrm{i}\left(\omega_n^{(\mathrm{in})} + \omega_m^{(\mathrm{out})}\right) T_0} \Psi_5(x) + A_n \bar{B}_m e^{\mathrm{i}\left(\omega_n^{(\mathrm{in})} - \omega_m^{(\mathrm{out})}\right) T_0} \Psi_6(x) + cc.
\end{aligned}
\tag{20}
$$

where the in-plane shape functions $\Psi_k(x)$, $k = 1, 2, 3, 4$ and out-of-plane ones $\Psi_k(x)$, $k = 5, 6$, are governed by the linear boundary value problems (BVPs)

$$
-4\left(\omega_n^{(\mathrm{in})}\right)^2 \Psi_1(x) + L_w(\Psi_1(x)) = \Pi_1(x)
\tag{21}
$$

$$
L_w(\Psi_2(x)) = \Pi_2(x)
\tag{22}
$$

$$
-4\left(\omega_m^{(\mathrm{out})}\right)^2 \Psi_3(x) + L_w(\Psi_3(x)) = \Pi_3(x)
\tag{23}
$$

$$
L_w(\Psi_4(x)) = \Pi_4(x)
\tag{24}
$$

$$
-\left(\omega_n^{(\mathrm{in})} + \omega_m^{(\mathrm{out})}\right)^2 \Psi_5(x) + L_v(\Psi_5(x)) = \Pi_5(x)
\tag{25}
$$

$$
-\left(\omega_n^{(\mathrm{in})} - \omega_m^{(\mathrm{out})}\right)^2 \Psi_6(x) + L_v(\Psi_6(x)) = \Pi_6(x)
\tag{26}
$$

Here the linear differential (integral) operators L_w, L_v are defined in Eq. (5). These linear BVPs can be solved by the standard method for linear integral-differential or differential equations [30], and illustrations of typical shape functions $\Psi_i(x)$ are presented in "Appendix 3".

Consider one-to-one resonant interaction/coupling between the in-plane mode and out-of-plane mode, and assume out-of-plane primary resonant boundary/support excitation

$$
\omega_n^{(\mathrm{in})} = \omega_m^{(\mathrm{out})} + \varepsilon^2 \sigma_1, \quad \Omega = \omega_m^{(\mathrm{out})} + \varepsilon^2 \sigma_2
\tag{27}
$$

where σ_1 and σ_2 are two detuning parameters. Thus the non-homogeneous 3rd-order resonant boundary conditions in Eq. (14) are rewritten as

$$
\begin{aligned}
v_3(x, t) &= e^{\mathrm{i}\omega_m^{(\mathrm{out})} T_0} e^{-\mathrm{i}\theta_0} \frac{Z_0 e^{\mathrm{i}\sigma_2 T_2}}{2} + cc., \quad q_3(x, t) = i\Omega v_3 \quad at \; x = 0 \\
v_3(x, t) &= e^{\mathrm{i}\omega_m^{(\mathrm{out})} T_0} \frac{Z_0 e^{\mathrm{i}\sigma_2 T_2}}{2} + cc., \quad q_3(x, t) = i\Omega v_3 \qquad at \; x = 1
\end{aligned}
\tag{28}
$$

Substituting the 1st-order solutions in Eq. (17) and 2nd-order solutions in Eq. (20) into the 3rd-order equations in Eq. (13), using Eq. (27), we obtain the 3rd-order in-plane equations

$$
\begin{aligned}
D_0 w_3 - p_3 &= -D_2 A_n \phi_n e^{\mathrm{i}\omega_n^{(\mathrm{in})} T_0} + cc. \\
D_0 p_3 + L_w(w_3) &= -\mathrm{i}\omega_n (D_2 A_n + 2c A_n) \phi_n e^{\mathrm{i}\omega_n^{(\mathrm{in})} T_0} + A_n |A_n|^2 \chi_1(x) e^{\mathrm{i}\omega_n^{(\mathrm{in})} T_0} \\
&\quad + A_n |B_m|^2 \chi_2(x) e^{\mathrm{i}\omega_n^{(\mathrm{in})} T_0} + \bar{A}_n B_m^2 \chi_3(x) e^{\mathrm{i}\left(2\omega_m^{(\mathrm{out})} - \omega_n^{(\mathrm{in})}\right) T_0} + \mathrm{NST}_3. + cc.
\end{aligned}
\tag{29}
$$

and the 3rd-order out-of-plane equations

$$D_0 v_3 - q_3 = -D_2 B_m \varphi_m e^{\mathrm{i}\omega_m^{(\text{out})} T_0} + cc.$$

$$D_0 q_3 + L_v (v_3) = -\mathrm{i}\omega_m (D_2 B_m + 2c B_m) \varphi_m e^{\mathrm{i}\omega_m^{(\text{out})} T_0} + B_m |B_m|^2 \chi_4 (x) e^{\mathrm{i}\omega_m^{(\text{out})} T_0} \qquad (30)$$

$$+ B_m |A_n|^2 \chi_5 (x) e^{\mathrm{i}\omega_m^{(\text{out})} T_0} + \bar{B}_m A_n^2 \chi_6 (x) e^{\mathrm{i}\left(2\omega_n^{(\text{in})} - \omega_m^{(\text{out})}\right) T_0} + \text{NST}_4. + cc.$$

where the coefficients $\chi_k(x)$, $k = 1, 2, \ldots, 6$, are presented in "Appendix 2", and NST_3 and NST_4 denote the non-secular terms.

3.2 Solvability conditions: multiple resonant boundary modulations

The above multiple scale expansion is similar to the cable dynamics under in-plane distributed excitations with fixed supports [32,33]. We point out that the main difficulty lies in the solvability conditions for Eqs. (29) and (30), noting the two resonant boundary conditions in Eqs. (28). In most references, the approach used to derive the solvability conditions is designed for resonant distributed external excitations(with fixed supports), which is not suitable for the present localized boundary excitations (with moving supports). To tackle the two non-homogeneous resonant boundary conditions in Eq. (28), we try to extend the boundary modulation approach formulated by the authors in Ref. [22].

Multiply the right-hand sides of Eqs. (29) and (30) by the adjoint solutions [33] $\boldsymbol{q}_w^\dagger = \left[\mathrm{i}\omega_k^{(\text{in})}, 1\right]\phi_k(x)$ $e^{-\mathrm{i}\omega_k^{(\text{in})} T_0}$ and $\boldsymbol{q}_v^\dagger = \left[\mathrm{i}\omega_k^{(\text{out})}, 1\right]\varphi_k(x) e^{-\mathrm{i}\omega_k^{(\text{out})} T_0}$, respectively, and then integrate in the domain $[0, 1] \times [0, \tau_0]$, where τ_0 is the period of w_3 and v_3 with respect to T_0. We thus obtain the right-hand sides (RHS) as

$$\text{RHS}^{(\text{in})} = \left\{-2\mathrm{i}\omega_n^{(\text{in})} (D_2 A_n + \mu_n A_n) + \Gamma_1 A_n |A_n|^2 + \Gamma_2 A_n |B_m|^2 + \Gamma_3 \bar{A}_n B_m^2 e^{-2\mathrm{i}\sigma_1 T_2}\right\} \tau_0 \delta_{nk} \qquad (31)$$

$$\text{RHS}^{(\text{out})} = \left\{-2\mathrm{i}\omega_m^{(\text{out})} (D_2 B_m + \mu_n B_m) + \Gamma_4 B_m |B_m|^2 + \Gamma_5 B_m |A_n|^2 + \Gamma_6 \bar{B}_m A_n^2 e^{2\mathrm{i}\sigma_1 T_2}\right\} \tau_0 \delta_{mk} \qquad (32)$$

where the Kronecker delta $\delta_{nk} = 1$, $n = k$; $\delta_{nk} = 0$, $n \neq k$ and the (3rd-order) nonlinear interaction coefficient $\Gamma_n, \Gamma_{nm}, \Gamma_m, \Gamma_{mn}$ are

$$\Gamma_k = \langle \phi_n, \chi_k(x) \rangle, \; k = 1, 2, 3, \quad \mu_n = \left\langle c(x), \; \phi_n^2 \right\rangle$$
$$\Gamma_k = \langle \varphi_m, \chi_k(x) \rangle, \; k = 4, 5, 6, \quad \mu_m = \left\langle c(x), \; \varphi_m^2 \right\rangle \qquad (33)$$

if introducing an inner product for any two smooth functions $\psi_1(x)$ and $\psi_2(x)$

$$\langle \psi_1, \psi_2 \rangle = \int_0^1 \bar{\psi}_1(x) \; \psi_2(x) \, \mathrm{d}x \qquad (34)$$

To use the boundary modulation approach formulated in Ref. [22], the followings are key steps. Multiplying the left-hand sides of Eqs. (29) and (30) by the adjoint solutions $\boldsymbol{q}_w^\dagger = \left[\mathrm{i}\omega_k^{(\text{in})}, 1\right]\phi_k(x) e^{-\mathrm{i}\omega_k^{(\text{in})} T_0}$ and $\boldsymbol{q}_v^\dagger = \left[\mathrm{i}\omega_k^{(\text{out})}, 1\right]\varphi_k(x) e^{-\mathrm{i}\omega_k^{(\text{out})} T_0}$, and then integrating in the domain $[0, 1] \times [0, \tau_0]$, we obtain the left-hand sides (LHS), explicitly

$$\text{LHS}^{(\text{in})} = 0 \qquad (35)$$

$$\text{LHS}^{(\text{out})} = \int_0^{\tau_0} \int_0^1 \left\{ \mathrm{i}\omega_k^{(\text{out})} \varphi_k e^{-\mathrm{i}\omega_k^{(\text{out})} T_0} (D_0 v_3 - q_3) + \varphi_k e^{-\mathrm{i}\omega_k^{(\text{out})} T_0} (D_0 q_3 + L_v(v_3)) \right\} \mathrm{d}x \mathrm{d}T_0$$

$$= -\int_0^{\tau_0} \int_0^1 \underbrace{\left[D_0 \left(\varphi_k(x) e^{\mathrm{i}\omega_k^{(\text{out})} T_0} \right) - \mathrm{i}\omega_k \varphi_k(x) e^{\mathrm{i}\omega_k^{(\text{out})} T_0} \right]}_{=0} \cdot q_3 \mathrm{d}x \mathrm{d}T_0$$

$$+ \int_0^{\tau_0} \int_0^1 \underbrace{\left[D_0 \left(\mathrm{i}\omega_k^{(\text{out})} \varphi_k(x) e^{\mathrm{i}\omega_k^{(\text{out})} T_0} \right) + L_v \left[\varphi_k(x) e^{\mathrm{i}\omega_k^{(\text{out})} T_0} \right] \right]}_{=0} \cdot v_3 \mathrm{d}x \mathrm{d}T_0 + \text{BT} \qquad (36)$$

$$= \text{BT} \neq 0$$

where the nonzero "boundary terms" (BT) are caused by the 3rd-order resonant boundary conditions denoted by Eq. (28), which are due to the out-of-plane support motions. There are no boundary terms for the in-plane dynamics. Integration by parts is used, and the over-bar means complex conjugate manipulations. The integrals marked by the brace are equal to zero as they are actually the 1st-order linear dynamics denoted by Eq. (9).

The above nonzero boundary terms BT for the out-of-plane motions are derived in the following. Noting the linear differential operator $L_v(v) = -v''$ in Eq. (5) and using integration by parts, we obtain

$$
\begin{aligned}
&\int_0^{\tau_0} \int_0^1 \varphi_k(x) e^{-\mathrm{i}\omega_k^{(\text{out})} T_0} L_v(v_3) \mathrm{d}x \mathrm{d}T_0 \\
&= \int_0^{\tau_0} \left(\varphi_k'(x) v_3 \right)\big|_0^1 e^{-\mathrm{i}\omega_k^{(\text{out})} T_0} \mathrm{d}T_0 - \int_0^{\tau_0} \int_0^1 \left(\varphi_k e^{-\mathrm{i}\omega_k^{(\text{out})} T_0} \right)'' \cdot v_3 \mathrm{d}x \mathrm{d}T_0 \\
&= \underbrace{- e^{-\mathrm{i}\theta_0} \varphi_k'(0) \frac{Z_0}{2} e^{\mathrm{i}\sigma_2 T_2} \tau_0 \delta_{mk}}_{\text{BT}_0} + \underbrace{\varphi_k'(1) \frac{Z_0}{2} e^{\mathrm{i}\sigma_2 T_2} \tau_0 \delta_{mk}}_{\text{BT}_1} \\
&\quad + \int_0^{\tau_0} \int_0^1 L_v \left(\varphi_k(x) e^{-\mathrm{i}\omega_k^{(\text{out})} T_0} \right) v_3 \mathrm{d}x \mathrm{d}T_0
\end{aligned}
\tag{37}
$$

where $\text{BT}_0 + \text{BT}_1 = \text{BT}$ are the nonzero boundary terms caused by the two moving supports, and the Kronecker $\delta_{mk} = 1$ for $m = k$, otherwise $\delta_{mk} = 0$. The resonant boundary conditions due to support motions, i.e. Eq. (28), are used in the last equality above. One notes that the phase lag between support motions, i.e. θ_0, is naturally included in the above boundary modulation terms.

Thus, the dynamic effects caused by the moving supports can be characterized by two boundary dynamic coefficients $\Lambda_{k0}, \Lambda_{k1}$

$$
\Lambda_{k0} = -\varphi_k'(0), \quad \Lambda_{k1} = \varphi_k'(1)
\tag{38}
$$

Therefore, the nonzero boundary terms BT caused by the resonant support motions are written as

$$
\text{LHS}^{(\text{out})} = \text{BT} = \left(e^{-\mathrm{i}\theta_0} \Lambda_{k0} + \Lambda_{k1} \right) \frac{Z_0}{2} e^{\mathrm{i}\sigma_2 T_1} \tau_0 \delta_{mk}
\tag{39}
$$

Letting LHS = RHS (in-plane and out-of-plane, respectively), we obtain cable's modulation equations for one-to-one resonant coupled dynamics under asynchronous support motions

$$
D_2 A_n = -\mu_n A_n - \frac{\mathrm{i}}{2\omega_n^{(\text{in})}} \left(\Gamma_1 A_n |A_n|^2 + \Gamma_2 A_n |B_m|^2 + \Gamma_3 \bar{A}_n B_m^2 e^{-2\mathrm{i}\sigma_1 T_2} \right)
\tag{40}
$$

$$
\begin{aligned}
D_2 B_m &= -\mu_m B_m - \frac{\mathrm{i}}{2\omega_m^{(\text{out})}} \left(\Gamma_4 B_m |B_m|^2 + \Gamma_5 B_m |A_n|^2 + \Gamma_6 \bar{B}_m A_n^2 e^{2\mathrm{i}\sigma_1 T_2} \right) \\
&\quad + \mathrm{i} \frac{e^{-\mathrm{i}\theta_0} \Lambda_{k0} + \Lambda_{k1}}{4\omega_m^{(\text{out})}} Z_0 e^{\mathrm{i}\sigma_2 T_2} \delta_{mk}
\end{aligned}
\tag{41}
$$

We point out that for the symmetric out-of-plane modes, i.e. $\phi_k(x)$, k is odd, the two boundary dynamic coefficients defined in Eq. (38) are exactly equal to each other. For asymmetric modes, however, they are opposite.

4 Dynamic analysis and nonlinear responses

4.1 Modulation equations in a polar form

For further dynamic analysis, we introduce the following transformations [24]

$$
A_n(T_2) = \frac{1}{2} a_n(T_2) e^{\mathrm{i}\alpha_n(T_2)}, \quad B_m(T_2) = \frac{1}{2} b_m(T_2) e^{\mathrm{i}\beta_m(T_2)}
\tag{42}
$$

and substitute them into Eqs. (40) and (41). Noting $\Lambda_{k0} = \Lambda_{k1} = \Lambda_m$ for symmetric out-of-plane modes, we obtain the amplitude equations

$$
a_n' = -\mu_n a_n + \frac{1}{8\omega_n^{(\text{in})}} \Gamma_3 a_n b_m^2 \sin(\gamma_1)
\tag{43}
$$

Table 1 Cable's boundary dynamic coefficients and nonlinear interaction coefficients: 1:1 resonant coupled dynamics ($\alpha = 434.286$, $f = 0.004$, 0.009, $\Omega = \omega_{\mathrm{m}} + \varepsilon^2\sigma_2$)

Coefficients	$\lambda = 0.2\pi\,(\sigma_1 = 0.0505)$	$\lambda = 0.5\pi\,(\sigma_1 = 0.3026)$
Λ_{m}	$-\sqrt{2}\pi$	$-\sqrt{2}\pi$
Γ_1	$-53{,}693.8$	$-10{,}248.9$
Γ_2	$-38{,}383.5$	$-20{,}988.8$
Γ_3	$-21{,}874.0$	$-25{,}667.2$
Γ_4	$-62{,}321.3$	$-57{,}650.4$
Γ_5	$-37{,}458.5$	$-14{,}903.0$
Γ_6	$-20{,}471.4$	$-16{,}038.4$

Fig. 2 Cable's typical frequency responses under asynchronous support excitations: $\sigma_1 = 0.0505$, $Z_0 = 0.001$, $\theta_0 = 0.2\pi$

$$b_m' = -\mu_m b_m - \frac{1}{8\omega_m^{(\mathrm{out})}}\Gamma_6 b_m a_n^2 \sin(\gamma_1) - \frac{\Lambda_m}{\omega_m^{(\mathrm{out})}}Z_0 \cos\left(\frac{\theta_0}{2}\right)\sin\left(\gamma_2 - \frac{\theta_0}{2}\right) \tag{44}$$

and the (relative) phase equations

$$\gamma_1' = -2\sigma_1 + \frac{\Gamma_1 a_n^2 + \Gamma_2 b_m^2 + \Gamma_3 b_m^2 \cos(\gamma_1)}{4\omega_n^{(\mathrm{in})}} \\ - \frac{\Gamma_4 b_m^2 + \Gamma_5 a_n^2 + \Gamma_6 a_n^2 \cos(\gamma_1)}{4\omega_m^{(\mathrm{out})}} + \frac{2\Lambda_m Z_0}{\omega_m^{(\mathrm{out})} b_m}\cos\left(\frac{\theta_0}{2}\right)\cos\left(\gamma_2 - \frac{\theta_0}{2}\right) \tag{45}$$

$$\gamma_2' = \sigma_2 + \frac{\Gamma_4 b_m^2 + \Gamma_5 a_n^2 + \Gamma_6 a_n^2 \cos(\gamma_1)}{8\omega_m^{(\mathrm{out})}} - \frac{\Lambda_m Z_0}{\omega_m^{(\mathrm{out})} b_m}\cos\left(\frac{\theta_0}{2}\right)\cos\left(\gamma_2 - \frac{\theta_0}{2}\right) \tag{46}$$
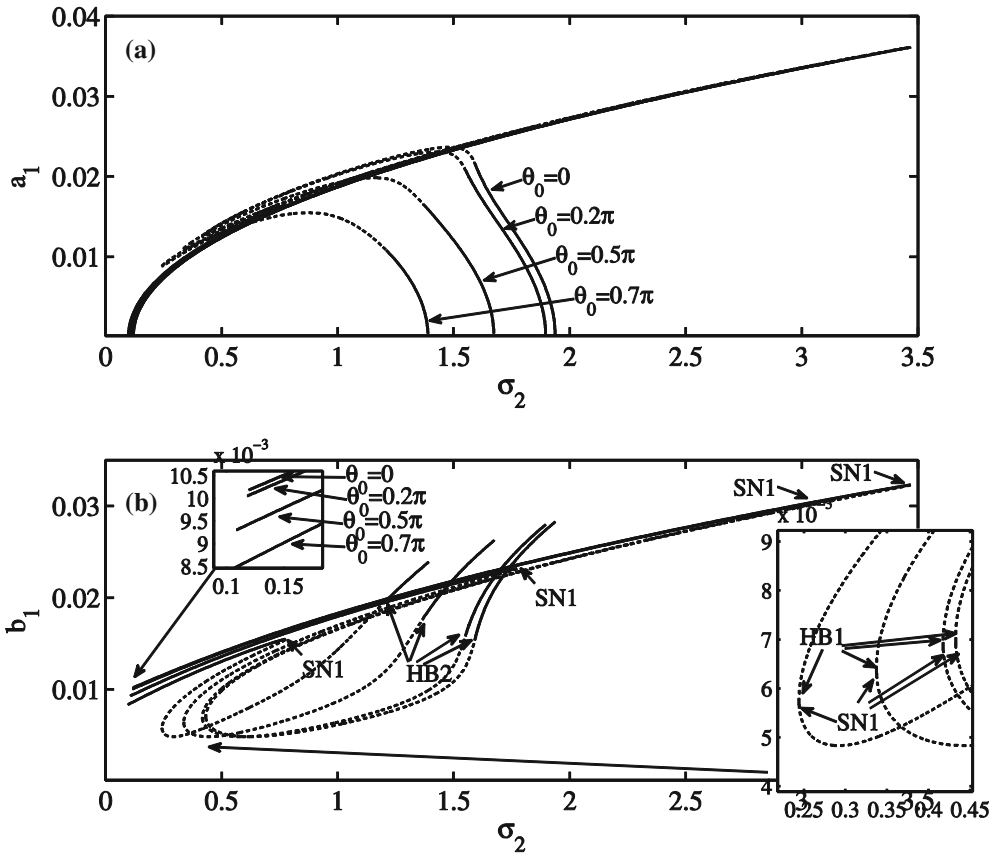
Fig. 3 Cable's typical frequency responses under asynchronous support excitations with varying phase lags: $\sigma_1 = 0.0505$, $Z_0 = 0.001$, $\theta_0 = 0, 0.2\pi, 0.5\pi, 0.7\pi$

where $\gamma_1 = 2\beta_m - 2\alpha_n - 2\sigma_1 T_2$, and $\gamma_2 = \sigma_2 T_2 - \beta_m$. Thus, solving Eqs. (43), (44), (45), and (46), we obtain cable's 2nd-order non-planar coupled responses as

$$w(x, t) = \varepsilon a_n \cos\left(\Omega t - \frac{\gamma_1}{2} - \gamma_2\right)\phi_n(x) + \frac{1}{2}\varepsilon^2 \left\{a_n^2 \cos\left(2\Omega t - \gamma_1 - 2\gamma_2\right)\Psi_1(x)\right.$$
$$\left. + a_n^2 \Psi_2(x) + b_m^2 \cos\left(2\Omega t - 2\gamma_2\right)\Psi_3(x) + b_m^2 \Psi_4(x)\right\} \cdots, \tag{47}$$

$$v(x, t) = \varepsilon b_m \cos\left(\Omega t - \gamma_2\right)\varphi_m(x) + \frac{1}{2}\varepsilon^2 a_n b_m \left\{\cos\left(2\Omega t - \frac{\gamma_1}{2} - 2\gamma_2\right)\Psi_5(x)\right.$$
$$\left. + \cos\left(-\frac{\gamma_1}{2}\right)\Psi_6(x)\right\} + \cdots, \tag{48}$$

We note that the cable's steady periodic oscillations correspond to steady-state solutions of the modulation equations/reduced dynamics. Thus, the steady-state solutions of Eqs. (43)–(46) would be fully investigated in the following. Setting $a_n' = b_m' = \gamma_1' = \gamma_2' = 0$ in the modulation equations, we obtain

$$0 = -\mu_n a_n + \frac{1}{8\omega_n^{(in)}}\Gamma_3 a_n b_m^2 \sin(\gamma_1) \tag{49}$$

$$0 = -\mu_m b_m - \frac{1}{8\omega_m^{(out)}}\Gamma_6 b_m a_n^2 \sin(\gamma_1) - \frac{\Lambda_m}{\omega_m^{(out)}}Z_0 \cos\left(\frac{\theta_0}{2}\right)\sin\left(\gamma_2 - \frac{\theta_0}{2}\right) \tag{50}$$

$$0 = -2\sigma_1 + \frac{\Gamma_1 a_n^2 + \Gamma_2 b_m^2 + \Gamma_3 b_m^2 \cos(\gamma_1)}{4\omega_n^{(in)}}$$

$$- \frac{\Gamma_4 b_m^2 + \Gamma_5 a_n^2 + \Gamma_6 a_n^2 \cos(\gamma_1)}{4\omega_m^{(out)}} + \frac{2\Lambda_m Z_0}{\omega_m^{(out)} b_m}\cos\left(\frac{\theta_0}{2}\right)\cos\left(\gamma_2 - \frac{\theta_0}{2}\right) \tag{51}$$
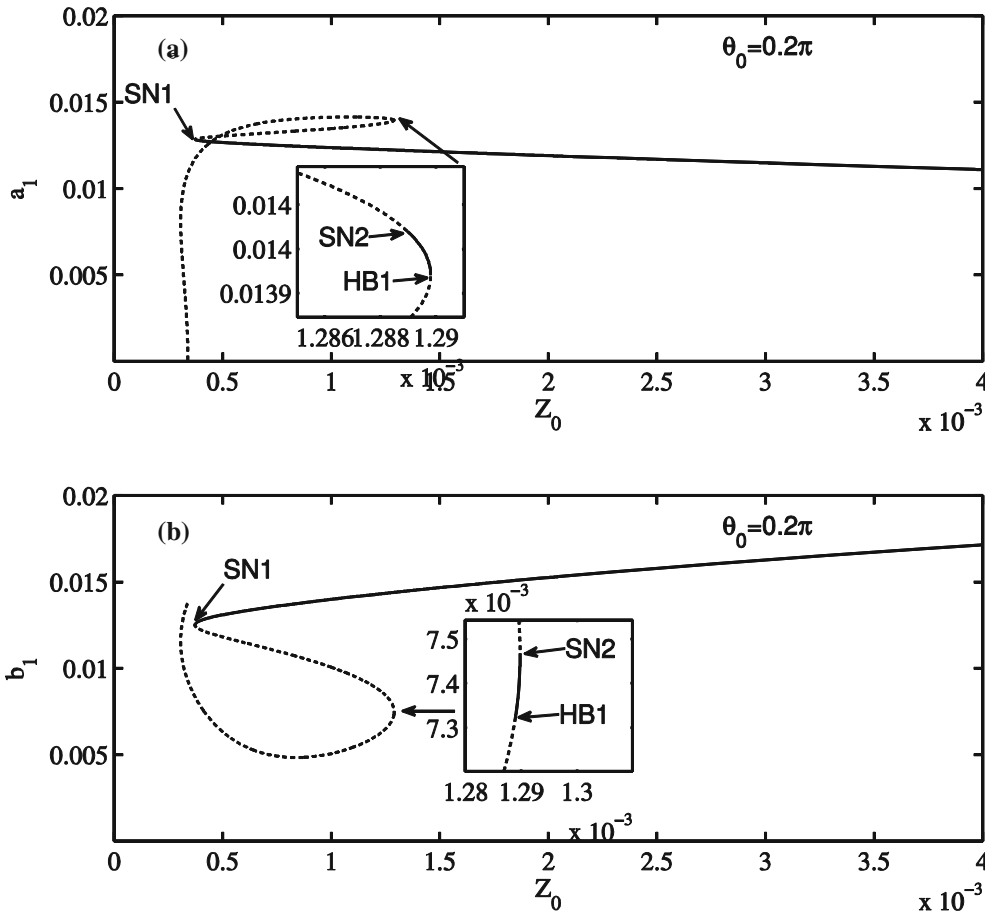
Fig. 4 Cable's typical amplitude (of support deflection) responses under asynchronous support excitations: $\sigma_1 = 0.0505, \sigma_2 = 0.5,$ $\theta_0 = 0.2\pi$

$$0 = \sigma_2 + \frac{\Gamma_4 b_m^2 + \Gamma_5 a_n^2 + \Gamma_6 a_n^2 \cos(\gamma_1)}{8\omega_m^{(out)}} - \frac{\Lambda_m Z_0}{\omega_m^{(out)} b_m} \cos\left(\frac{\theta_0}{2}\right) \cos\left(\gamma_2 - \frac{\theta_0}{2}\right) \tag{52}$$

Therefore, the steady-state solutions would be obtained by solving roots of the above equations, i.e. Eqs. (49)–(52).

4.2 Steady-state solutions and bifurcation analysis

For the followed numerical study, we calculate the boundary dynamic coefficients Λ_m and 1:1 resonant coupled coefficients Γ_k for two typical cable models: one is strongly coupled model with $\sigma_1 = 0.0505$, and the other one is a weakly coupled model with $\sigma_1 = 0.3026$. The corresponding results are presented in Table 1 (the shape functions $\Psi_k(x)$ are presented in "Appendix 3").

Using the Newton–Raphson algorithm (combined with the homotopic algorithm to reduce the sensitivity to initial guesses) for solving the roots of Eqs. (49)–(52), we obtain the steady-state solutions, which correspond to cable's steady periodic oscillations. These steady-state solutions are then used as initial values for the pseudo arc-length method [34], a numerical continuation algorithm, and the frequency or amplitude (of support deflection) response diagrams are constructed by sweeping the excitation frequency Ω or the amplitude Z_0. In the following, solid lines denote stable steady-state solutions and dotted lines denote unstable ones, and this is determined by checking the eigenvalues of the modulation equations' Jacobi matrix [24]. SN and HB are short for saddle-node bifurcations and Hopf bifurcations, respectively. Note that only non-planar coupled steady-state solutions are depicted.
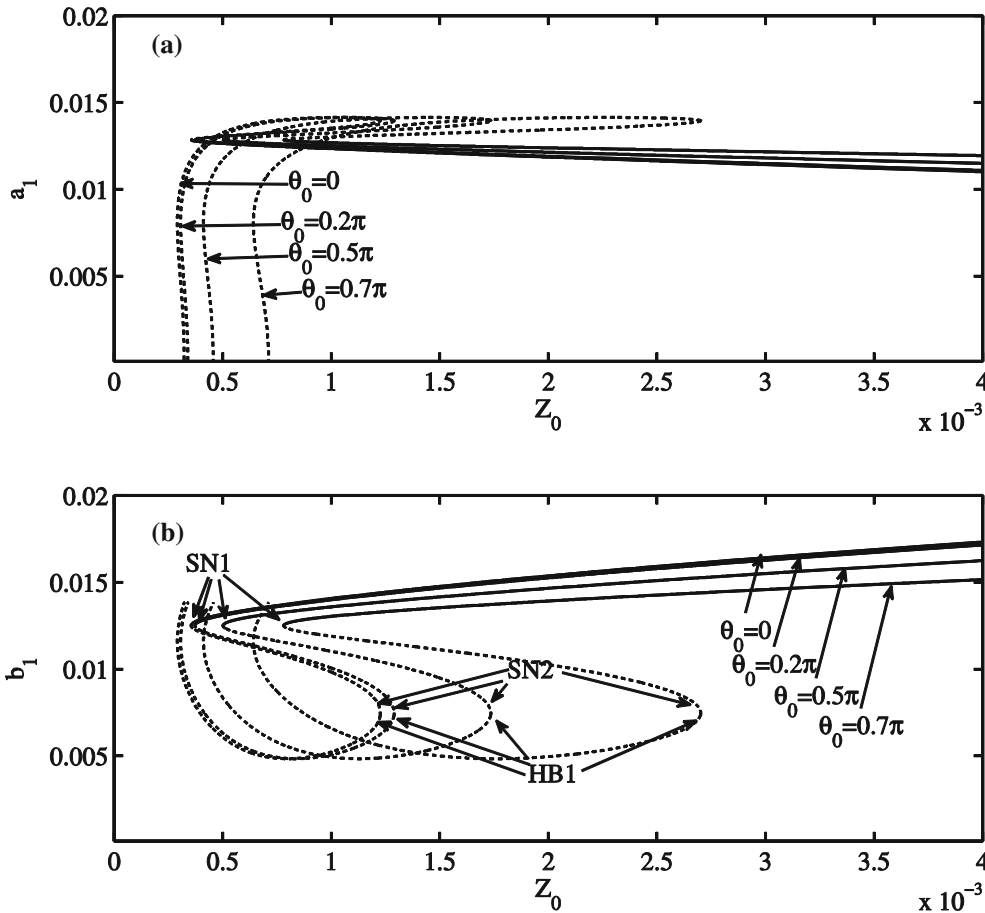
Fig. 5 Cable's typical amplitude responses under asynchronous support excitations with varying phase lags: $\sigma_1 = 0.0505$, $\sigma_2 =,$ $\theta_0 = 0, 0.2\pi, 0.5\pi, 0.7\pi$

For cable's non-planar coupled motions under asynchronous support excitations, the typical frequency response diagrams are depicted in Fig. 2 and the phase lag is $\theta_0 = 0.2\pi$. With a fixed detuning parameter $\sigma_1 = 0.0505$, the in-plane and out-of-plane components are presented in subplots (a) and (b), respectively. As the detuning parameter σ_2 is swept forward, the stable coupled steady-state solutions, initiated at $\sigma_2 = 0.1182$, turn unstable through a saddle-node bifurcation at SN1 and then become stable at the saddle-node bifurcation point SN2 with σ_2 reversely swept. Furthermore, the steady-state solutions lose stability through a Hopf bifurcation at HB1 and regain stability through a reverse Hopf bifurcation at HB2, before finally ending at $\sigma_2 = 1.8960$.

For a further understanding of phase lag's effect on coupled responses, we present four typical frequency response diagrams by varying the phase lag θ_0, i.e. $\theta_0 = 0, 0.2\pi, 0.5\pi, 0.7\pi$. As illustrated in Fig. 3, the response peaks, i.e. $\max(a_1)$ and $\max(b_1)$, decrease as the phase lag θ_0 is increased. We point out that this peak-reduction effect is mainly due to the excitation reduced factor $\cos(\theta_0/2)$ in Eqs. (44)–(46), which is closely associated with the fact that the two boundary dynamic coefficients introduced in Eqs. (38) are equal to each other for symmetric out-of-plane support motions. At the same time, the parameter domains where coupled responses exist also shrink. Furthermore, we note that, with the phases θ_0 increased, all the bifurcations, i.e. SN1, SN2, HB1, and HB2, occur earlier with smaller detuning parameters σ_2 . Roughly, a smaller σ_2 means a more resonant boundary excitation. Thus we conclude that, to activate the bifurcations, more resonant boundary excitations are demanded for larger phase lags.

Typical amplitude (of support deflection) response diagrams for cable's coupled dynamics under asynchronous support motions are presented in Fig. 4, with a phase lag $\theta_0 = 0.2\pi$. As the amplitude of support motions Z_0 decreased, the stable coupled steady-state solutions turn unstable through a saddle-node bifurcation at SN1. The unstable solutions regain stability at the saddle-node bifurcation point SN2 and become unstable soon through a Hopf bifurcation at HB1. If Z_0 is too small, as illustrated in Fig. 4, coupled solutions vanish.
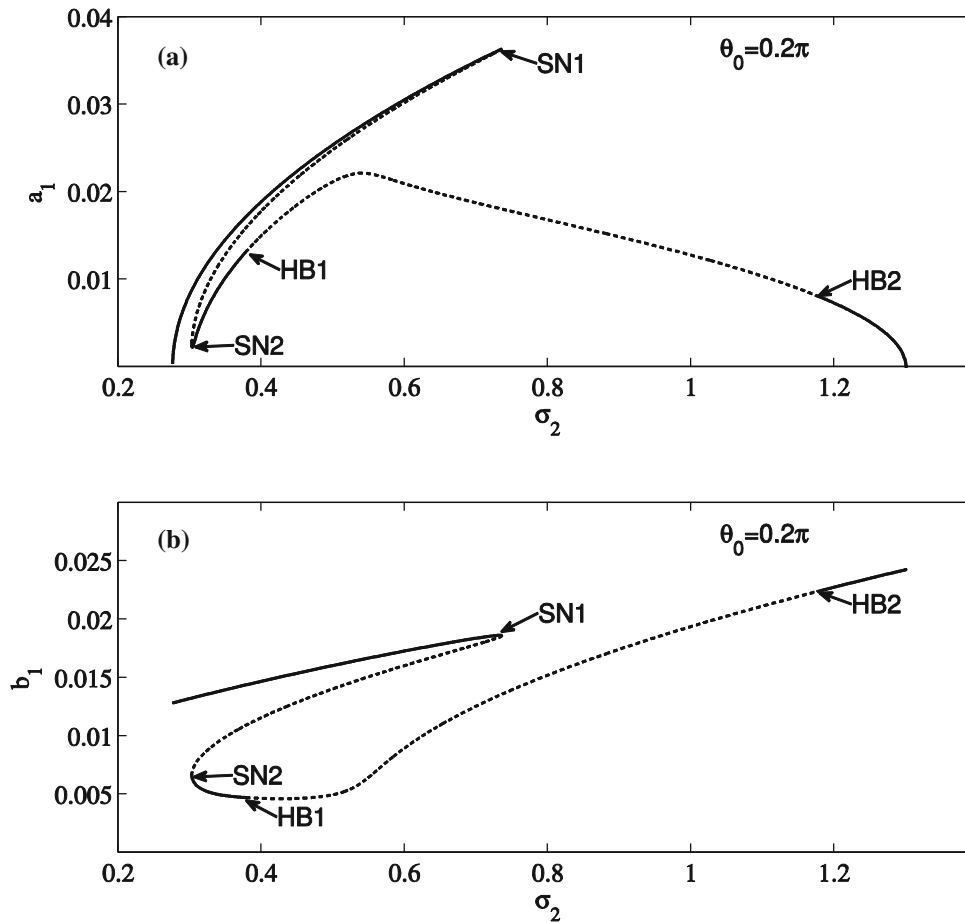
Fig. 6 Cable's typical frequency responses under asynchronous support excitations: $\sigma_1 = 0.3026$, $Z_0 = 0.001$, $\theta_0 = 0.2\pi$

Furthermore, by varying the phase lag θ_0, i.e. $\theta_0 = 0$, 0.2π, 0.5π, 0.7π, we intend to evaluate the effect of the phase lag on cable's coupled dynamics. The results are presented in Fig. 5. Again, the increasing phase lags θ_0 reduce the amplitude(of support deflection) response's peak magnitudes, as illustrated in Fig. 5. We also note that, with the phase lag θ_0 increased, all the bifurcations, i.e. SN1, SN2 and HB1, are retarded, meaning that they occur later with larger excitation amplitudes Z_0. Roughly, large excitation amplitudes Z_0 mean stronger excitations. Thus, equivalent to the frequency response diagrams in Fig. 3, we propose that the cable system with a larger phase lag would demand a more stronger support excitation to activate the associated bifurcations.

Another cable model with a larger detuning parameter $\sigma_1 = 0.3026$ is considered in the following. Physically, this cable is less resonant or more weakly coupled than the first one, i.e. $\sigma_1 = 0.0505$. Typical frequency responses for cable's non-planar coupled dynamics under asynchronous support excitations are presented in Fig. 6, with a phase lag $\theta_0 = 0.2\pi$. As the detuning parameter σ_2 increases from the bottom $\sigma_2 = 0.2759$, the stable coupled steady-state solutions turn unstable through a saddle-node bifurcation at SN1 and become stable at another saddle-node bifurcation point SN2, before losing stability through a Hopf bifurcation at HB1. The unstable coupled solutions regain stability through a reverse Hopf bifurcation at HB2 and end finally at $\sigma_2 = 1.3010$.

Again, as illustrated in Fig. 7, we attempt to vary the phase lag θ_0, i.e. $\theta_0 = 0$, 0.2π, 0.5π, 0.7π, to investigate the effect of the phase lag on cable's coupled frequency responses. The aforementioned peak magnitude-reduction effect, i.e. the increasing phase lag θ_0 tends to reduce the peak amplitude of the stable coupled responses, is confirmed again in Fig. 7. Besides those, we note two more interesting phenomena in the present less resonant coupled cable. The first is that the coupled solutions split into two disconnected branches if the phase lag θ_0 is increased from $\theta_0 = 0.2\pi$ to $\theta_0 = 0.5\pi$ or 0.7π. Even more, for $\theta_0 = 0.7\pi$, as the associated two branches of the coupled solutions are disconnected/disjoint further, our numerical results indicate that there is an uncoupled single-mode solution domain in between, i.e. $0.4091 < \sigma_2 < 0.5318$. And
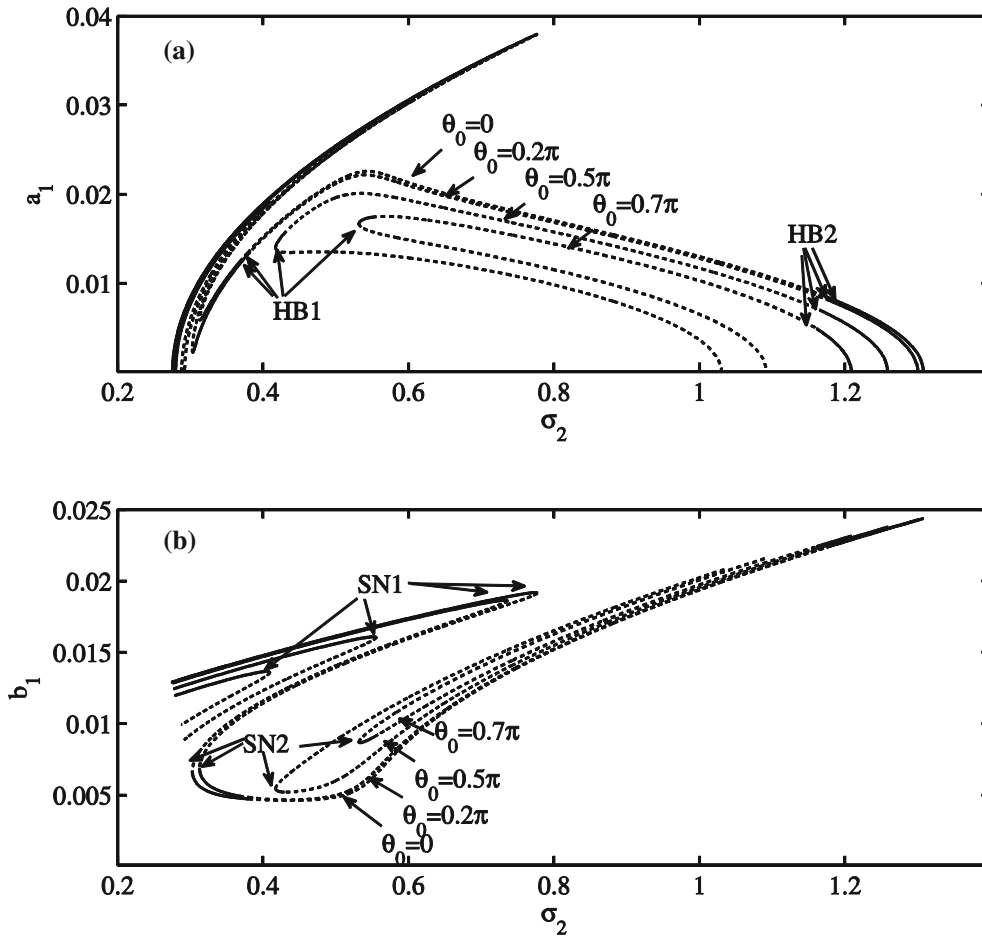
Fig. 7 Cable's typical frequency responses under asynchronous support excitations with varying phase lags: $\sigma_1 = 0.3026$, $Z_0 = 0.001$, $\theta_0 = 0, 0.2\pi, 0.5\pi, 0.7\pi$

the other new finding is about the bifurcation characteristics. We note that the saddle-node bifurcation SN1 on the left branches, similar to the strongly coupled cable, would occur with smaller detuning parameters σ_2 (or more resonant excitations) if the phase lag θ_0 is increased. However, the other bifurcations, falling on or approaching the right branches, tend to be activated by a larger σ_2 (or less resonant excitations) if the phase lag θ_0 increases.

Typical amplitude(of support deflection) response diagrams for the more weakly coupled cable model ($\sigma_1 = 0.3026$) are depicted in Fig. 8, with a phase lag $\theta_0 = 0.2\pi$. In contrast to the first cable model ($\sigma_1 = 0.0505$) with the same phase lag, one difference is notable. Explicitly, with the excitation amplitude Z_0 decreased, the stable coupled responses, after turning unstable at SN1, regaining stability at SN2, and becoming unstable at HB1, two more bifurcations occur, i.e. regaining stability through a Hopf bifurcation at HB2 and finally turning into unstable ones through a saddle-node bifurcation at SN3. In other words, a new stable solution branch exists in between.

The phase lag's effect on the amplitude (of support deflection) response diagrams are illustrated in Fig. 9, with varying phase lags. For $\theta_0 = 0, 0.2\pi, 0.5\pi$, the stable response amplitudes are reduced and the bifurcations, i.e. SN1, SN2 and HB1, occur with larger excitation amplitudes Z_0 if the phase lag θ_0 is increased. This is similar to the first strongly coupled cable model with $\sigma_1 = 0.0505$. For $\theta_0 = 0.7\pi$, however, the situation totally changes, as illustrated in Fig. 9. Explicitly, the bifurcations HB1, SN2 and SN1 all disappear and the stable solution branch initiated from SN1 also vanishes. The only stable coupled steady-state solutions exist between SN3 and HB2. We point out that the reason that the case with $\theta_0 = 0.7\pi$ is so distinct from other cases, lies in the fact that no coupled solution is found with $\sigma_2 = 0.5$. Recall that, in Fig. 7, the coupled solutions are split into two disconnected branches for $\theta_0 = 0.7\pi$ and there is an uncoupled single-mode domain in between,
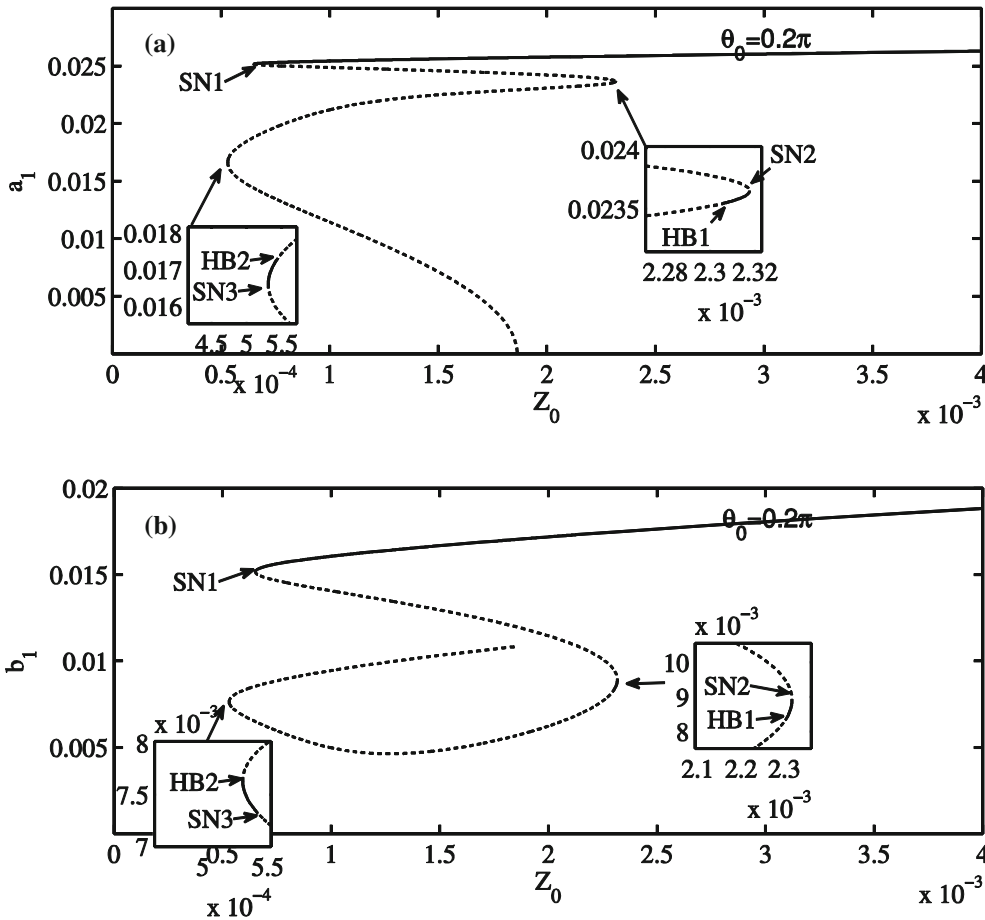
Fig. 8 Cable's typical amplitude (of support deflection) responses under asynchronous support excitations: $\sigma_1 = 0.3026, \sigma_2 = 0.5, \theta_0 = 0.2\pi$

i.e. $0.4091 < \sigma_2 < 0.5318$. Thus, the response diagrams for $\theta_0 = 0, 0.2\pi, 0.5\pi$ are continued from coupled solutions, while the diagram for $\theta_0 = 0.7\pi$ is continued from a single-mode solution.

5 Conclusions

A multi-scale modelling and analysis for cable's non-planar coupled dynamics under asynchronous out-of-plane support excitations is finished in this paper. Treating the small support motions as boundary perturbations, we derive cable's reduced coupled dynamic model, i.e. the modulation equations, through transforming the resonant support motions into boundary modulation terms by constructing the associated solvability conditions. Two boundary dynamic coefficients characterizing support's dynamic effect are derived, which are equal to each other for symmetric modes, while opposite for asymmetric modes. And the phase lag between supports is included roughly as a weight factor when summing the boundary effects of each support excitation. Thus the basic boundary modulation approach is extended to the multiple asynchronous supports.

Using this extended boundary modulation formulation, cable's non-planar one-to-one resonant coupled dynamics under multiple out-of-plane support motions with phase lags is fully investigated. The modulation equations' steady-state solutions, corresponding to cable's steady periodic oscillations, are solved and continued to construct the frequency and amplitude(of support deflection) response diagrams. Both the stability and bifurcation properties of the steady-state solutions are determined. By varying the phase lags, our numerical results demonstrate that, for the symmetric out-of-plane modes, the increasing phase lags between supports would reduce the coupled response's peak amplitudes and also tend to split one solution branch into two disjoint branches, especially for the weakly coupled cable. Furthermore, the cable system with a large phase lag would demand a more resonant (or stronger) support excitation to activate the associated bifurcations, except for those solutions being split into two branches.
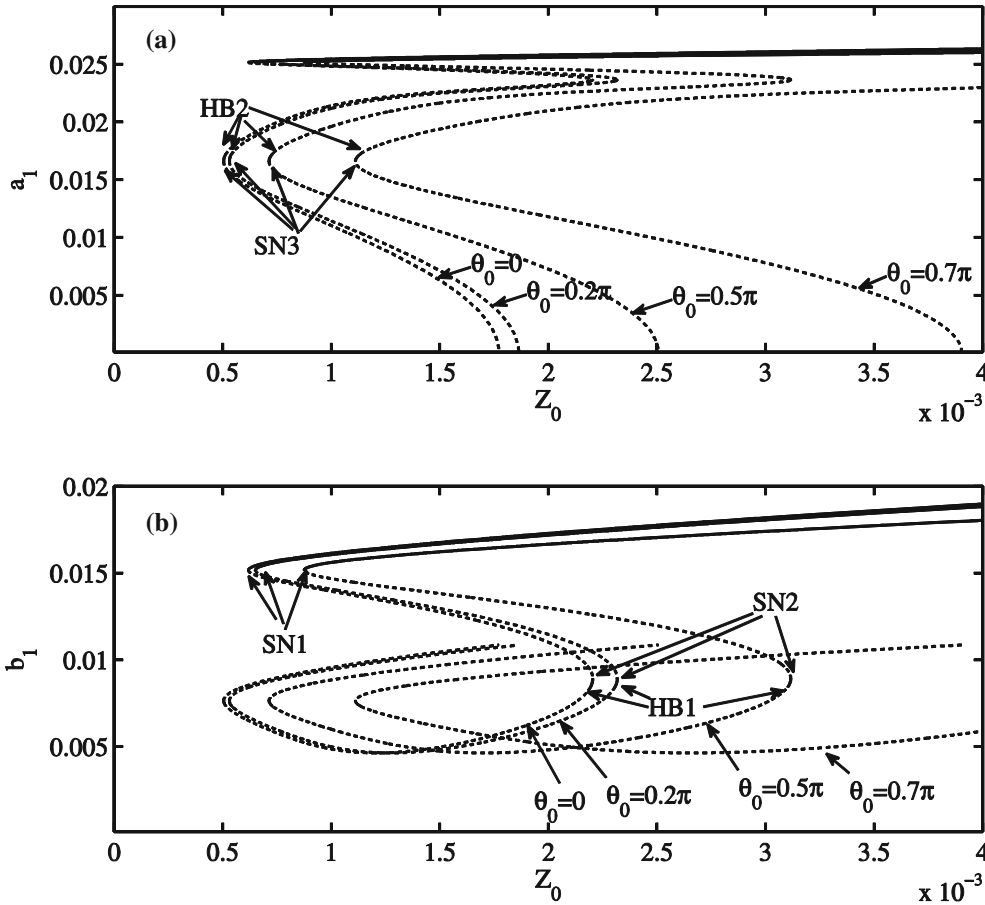
Fig. 9 Cable's typical amplitude responses under asynchronous support excitations with varying phase lags: $\sigma_1 = 0.3026$, $\sigma_2 = 0.5$, $\theta_0 = 0, 0.2\pi, 0.5\pi, 0.7\pi$

Appendix 1

The suspended cable's linear modal analysis can be found in references [3,30]. The in-plane symmetric modes are given by

$$\phi_n(x) = c_n \left[1 - \tan\left(\frac{\omega_n^{(in)}}{2} \right) \sin \omega_n^{(in)} x - \cos \omega_n^{(in)} x \right], \quad n = 1, 3, 5, \ldots \tag{53}$$

where c_i is the normalization constants. And the associated eigenfrequencies are determined by

$$\frac{1}{2} \omega_n^{(in)} - \tan\left(\frac{1}{2} \omega_n^{(in)} \right) - \frac{1}{2\lambda^2} \left(\omega_n^{(in)} \right)^3 = 0, \quad n = 1, 3, 5, \ldots \tag{54}$$

where $\lambda^2 = EA/mgl(8b/l)^3$ is the elasto-geometric parameter. The above nonlinear transcendental equations can be solved by the Newton–Raphson method.
The in-plane anti-symmetric modes are

$$\phi_n(x) = \sqrt{2} \sin(n\pi x), \quad n = 2, 4, 6, \ldots \tag{55}$$

with the associated eigenfrequencies as

$$\omega_n^{(in)} = n\pi, \quad n = 2, 4, 6, \ldots \tag{56}$$

And the out-of-plane modes are

$$\varphi_m(x) = \sqrt{2}\sin(m\pi x), \quad m = 1, 2, 3, \ldots \tag{57}$$

with the associated eigenfrequencies as

$$\omega_m^{(out)} = m\pi, \quad m = 1, 2, 3, \ldots \tag{58}$$

Appendix 2

$$\begin{aligned}
&\Pi_1(x) = \alpha/2 \langle \phi_n', \phi_n' \rangle y'' + \alpha \langle y', \phi_n' \rangle \phi_n'', \quad \Pi_3(x) = \alpha/2 \langle \varphi_m', \varphi_m' \rangle y'' \\
&\Pi_2(x) = \alpha/2 \langle \phi_n', \phi_n' \rangle y'' + \alpha \langle y', \phi_n' \rangle \phi_n'', \quad \Pi_4(x) = \alpha/2 \langle \varphi_m', \varphi_m' \rangle y''
\end{aligned} \tag{59}$$

$$\Pi_5(x) = \alpha \langle y', \phi_n' \rangle \varphi_m'', \quad \Pi_6(x) = \alpha \langle y', \phi_n' \rangle \varphi_m'' \tag{60}$$

$$\begin{aligned}
\chi_1(x) = &\frac{3\alpha}{2}\phi_n'' \langle \phi_n', \phi_n' \rangle + \alpha\phi_n'' \langle y', \Psi_1' \rangle + \alpha y'' \langle \phi_n', \Psi_1' \rangle + \alpha\Psi_1'' \langle y', \phi_n' \rangle \\
&+ 2\alpha\phi_n'' \langle y', \Psi_2' \rangle + 2\alpha y'' \langle \phi_n', \Psi_2' \rangle + 2\alpha\Psi_2'' \langle y', \phi_n' \rangle
\end{aligned} \tag{61}$$

$$\begin{aligned}
\chi_2(x) = &\alpha\phi_n'' \langle \varphi_m', \varphi_m' \rangle + 2\alpha\phi_n'' \langle y', \Psi_4' \rangle + 2\alpha y'' \langle \phi_n', \Psi_4' \rangle + 2\alpha\Psi_4'' \langle y', \phi_n' \rangle \\
&+ \alpha y'' \langle \varphi_m', \Psi_5' \rangle + \alpha y'' \langle \varphi_m', \Psi_6' \rangle
\end{aligned} \tag{62}$$

$$\chi_3(x) = \frac{\alpha}{2}\phi_n'' \langle \varphi_m', \varphi_m' \rangle + \alpha\phi_n'' \langle y', \Psi_3' \rangle + \alpha y'' \langle \phi_n', \Psi_3' \rangle + \alpha\Psi_3'' \langle y', \phi_n' \rangle + \alpha y'' \langle \varphi_m', \Psi_6' \rangle \tag{63}$$

$$\chi_4(x) = \frac{3\alpha}{2}\varphi_m'' \langle \varphi_m', \varphi_m' \rangle + \alpha\varphi_m'' \langle y', \Psi_3'(x) \rangle + 2\alpha\varphi_m'' \langle y', \Psi_4'(x) \rangle \tag{64}$$

$$\chi_5(x) = \alpha\varphi_m'' \langle \phi_n', \phi_n' \rangle + 2\alpha\varphi_m'' \langle y', \Psi_2' \rangle + \alpha\Psi_5'' \langle y', \phi_n' \rangle + \alpha\Psi_6'' \langle y', \phi_n' \rangle \tag{65}$$

$$\chi_6(x) = \frac{\alpha}{2}\varphi_m'' \langle \phi_n', \phi_n' \rangle + \alpha\varphi_m'' \langle y', \Psi_1' \rangle + \alpha\Psi_6'' \langle y', \phi_n' \rangle \tag{66}$$

Appendix 3

The shape functions $\Psi_k(x)$ are illustrated in the following, and they are used to calculate the nonlinear resonant interaction coefficients Γ_k (Fig. 10).
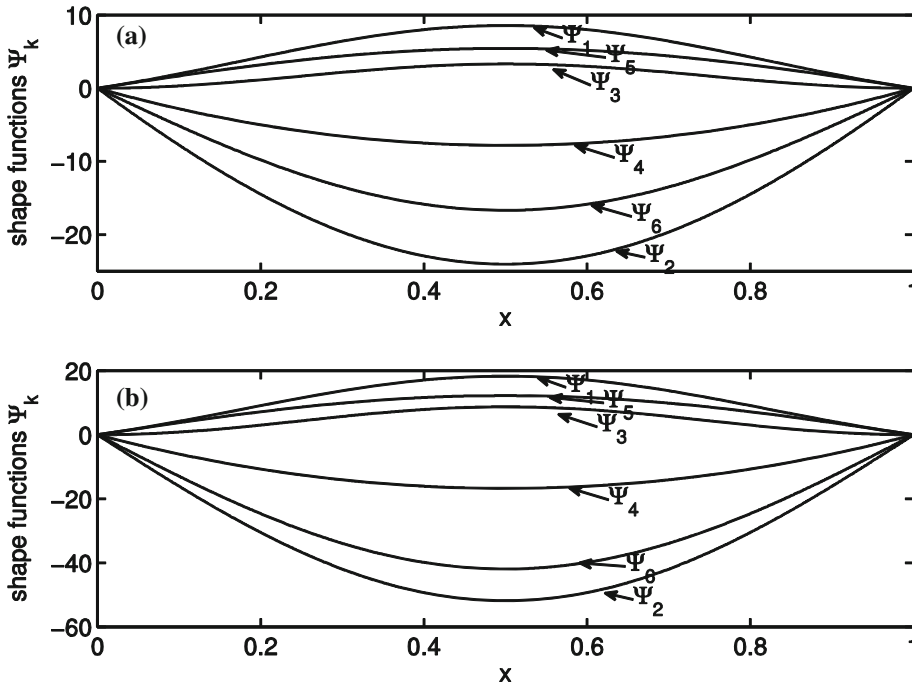

Fig. 10 Illustrations of the shape functions $\Psi_k(x)$, **a** cable model 1 with $\sigma_1 = 0.0505$, **b** cable model 2 with $\sigma_1 = 0.3026$

References

1. Rega, G.: Nonlinear vibrations of suspended cables—part I: modeling and analysis. Appl. Mech. Rev. **57**, 443–478 (2004)
2. Ibrahim, R.A.: Nonlinear vibrations of suspended cables—part III: random excitation and interaction with fluid flow. Appl. Mech. Rev. **57**, 515–549 (2004)
3. Irvine, H.M., Caughey, T.K.: The linear theory of free vibrations of a suspended cable. In: Proceedings of the Royal Society of London A: Mathematical, Physical and Engineering Sciences, pp. 299–315. The Royal Society (1974)
4. Irvine, H.M.: Cable Structures. Dover Publications, New York (1992)
5. Triantafyllou, M.: Dynamics of cables, towing cables and mooring systems. Shock Vib. Dig. **23**, 3–8 (1991)
6. Jin, D., Wen, H., Hu, H.: Modeling, dynamics and control of cable systems. Adv. Mech. **34**, 304–313 (2004)
7. Gattulli, V., Martinelli, L., Perotti, F., Vestroni, F.: Nonlinear oscillations of cables under harmonic loading using analytical and finite element models. Comp. Methods Appl. Mech. Eng. **193**, 69–85 (2004)
8. Xiong, W., Cai, C., Zhang, Y., Xiao, R.: Study of super long span cable-stayed bridges with CFRP components. Eng. Struct. **33**, 330–343 (2011)
9. Hagedorn, P., Schäfer, B.: On non-linear free vibrations of an elastic cable. Int. J. Non Linear Mech. **15**, 333–340 (1980)
10. Luongo, A., Rega, G., Vestroni, F.: Planar non-linear free vibrations of an elastic cable. Int. J. Non Linear Mech. **19**, 39–52 (1984)
11. Benedettini, F., Rega, G.: Non-linear dynamics of an elastic cable under planar excitation. Int. J. Non Linear Mech. **22**, 497–509 (1987)
12. Perkins, N.C.: Modal interactions in the non-linear response of elastic cables under parametric/external excitation. Int. J. Non Linear Mech. **27**, 233–250 (1992)
13. Benedettini, F., Rega, G., Alaggio, R.: Non-linear oscillations of a four-degree-of-freedom model of a suspended cable under multiple internal resonance conditions. J. Sound Vib. **182**, 775–798 (1995)
14. Cai, Y., Chen, S.: Dynamics of elastic cable under parametric and external resonances. J. Eng. Mech. **120**, 1786–1802 (1994)
15. Lilien, J.-L., Da Costa, A.P.: Vibration amplitudes caused by parametric excitation of cable stayed structures. J. Sound Vib. **174**, 69–90 (1994)
16. Costa, APd, Martins, J., Branco, F., Lilien, J.L.: Oscillations of bridge stay cables induced by periodic motions of deck and/or towers. J. Eng. Mech. **122**, 613–622 (1996)
17. El-Attar, M., Ghobarah, A., Aziz, T.: Non-linear cable response to multiple support periodic excitation. Eng. Struct. **22**, 1301–1312 (2000)
18. Berlioz, A., Lamarque, C.-H.: A non-linear model for the dynamics of an inclined cable. J. Sound Vib. **279**, 619–639 (2005)
19. Georgakis, C.T., Taylor, C.A.: Nonlinear dynamics of cable stays. Part 1: sinusoidal cable support excitation. J. Sound Vib. **281**, 537–564 (2005)
20. Wang, L., Zhao, Y.: Large amplitude motion mechanism and non-planar vibration character of stay cables subject to the support motions. J. Sound Vib. **327**, 121–133 (2009)
21. Gonzalez-Buelga, A., Neild, S., Wagg, D., Macdonald, J.: Modal stability of inclined cables subjected to vertical support excitation. J. Sound Vib. **318**, 565–579 (2008)
22. Guo, T.D., Kang, H.J., Wang, L.L.: A boundary modulation formulation for cable's non-planar coupled dynamics under out-of-plane support motion. Arch. Appl. Mech. (2015). doi:10.1007/s00419-015-1058-8
23. Shaw, S.W., Pierre, C.: Normal modes of vibration for non-linear continuous systems. J. Sound Vib. **169**, 319–347 (1994)
24. Nayfeh, A.H.: Nonlinear Interactions. Wiley, New York (2000)
25. Pakdemirli, M., Boyaci, H.: Effect of non-ideal boundary conditions on the vibrations of continuous systems. J. Sound Vib. **249**, 815–823 (2002)
26. Ghobarah, A., Aziz, T., El-Attar, M.: Response of transmission lines to multiple support excitation. Eng. Struct. **18**, 936–946 (1996)
27. Rega, G., Lacarbonara, W., Nayfeh, A., Chin, C.: Multiple resonances in suspended cables: direct versus reduced-order models. Int. J. Non Linear Mech. **34**, 901–924 (1999)
28. Nayfeh, A.H., Arafat, H.N., Chin, C.-M., Lacarbonara, W.: Multimode interactions in suspended cables. J. Vib. Control **8**, 337–387 (2002)
29. Lacarbonara, W.: Direct treatment and discretizations of non-linear spatially continuous systems. J. Sound Vib. **221**, 849–866 (1999)
30. Nayfeh, A.H., Pai, P.F.: Linear and Nonlinear Structural Mechanics. Wiley, New York (2008)
31. Srinil, N., Rega, G.: The effects of kinematic condensation on internally resonant forced vibrations of shallow horizontal cables. Int. J. Non Linear Mech. **42**, 180–195 (2007)
32. Pakdemirli, M., Nayfeh, S., Nayfeh, A.: Analysis of one-to-one autoparametric resonances in cables—discretization vs. direct treatment. Nonlinear Dyn. **8**, 65–83 (1995)
33. Lacarbonara, W., Rega, G., Nayfeh, A.: Resonant non-linear normal modes. Part I: analytical treatment for structural one-dimensional systems. Int. J. Non Linear Mech. **38**, 851–872 (2003)
34. Nayfeh, A.H., Balachandran, B.: Applied Nonlinear Dynamics: Analytical, Computational and Experimental Methods. Wiley, New York (2008)